

## Grafting of a rhenium-oxo complex on Schiff base functionalized graphene oxide: an efficient catalyst for the oxidation of amines†

Cite this: *Dalton Trans.*, 2014, **43**, 8054

Praveen K. Khatri,<sup>a</sup> Shivani Choudhary,<sup>a</sup> Raghuvir Singh,<sup>b</sup> Suman L. Jain\*<sup>a</sup> and Om P. Khatri\*<sup>a</sup>

A rhenium-oxo complex such as methyltrioxorhenium (MTO) has been homogeneously immobilized on a Schiff base modified graphene oxide (GrO) support *via* covalent bonding. The loading of MTO on GrO nanosheets was monitored by FTIR, TG-DTA, and elemental analyses. The developed heterogeneous catalyst is found to be efficient for the oxidation of various amines to the corresponding N-oxides using hydrogen peroxide as an oxidant in high to excellent yields. At the end of the reaction, the catalyst is readily recovered by filtration and reused for subsequent runs. After the third run, the catalyst showed a marginal decrease in catalytic activity owing to the leaching of the MTO complex from the support.

Received 6th December 2013,  
Accepted 10th March 2014

DOI: 10.1039/c3dt53421a

www.rsc.org/dalton

Graphene oxide (GrO), an oxidized form of graphene, has emerged as a promising material, particularly as a precursor to prepare reduced graphene oxide (rGrO), chemically functionalized graphene, and graphene based composite materials. Nonstoichiometric GrO possesses a crumpled and folded structure owing to the presence of sp<sup>3</sup> carbon and various defects.<sup>1,2</sup> Oxygen functionalities like hydroxyl, epoxy, carboxyl and carbonyl are placed on these sp<sup>3</sup> carbons within the basal planes and the edges of GrO sheets. These oxygen functionalities in GrO have been established as anchoring sites for chemical functionalization, nanoparticle immobilization, and blending with oligomers to prepare graphene-based polymeric composites, *etc.*<sup>1,2a,3,4</sup>

Recently, GrO has been recognized as a new low-cost carbocatalytic material with remarkable potential to facilitate various chemical transformations such as efficient conversion of various alcohols, alkenes, and alkynes into the corresponding aldehydes or ketones,<sup>5</sup> selective oxidation of thiols to disulfides, sulfides to sulfoxides,<sup>6</sup> alcohols to aldehydes or ketones,<sup>7,8</sup> aza-Michael addition of amines and electron deficient olefins to furnish the corresponding  $\beta$ -amino compounds,<sup>9</sup> and oxidative aromatization of 1,4-dihydropyridines into pyridine derivatives.<sup>10</sup> Owing to its high specific surface

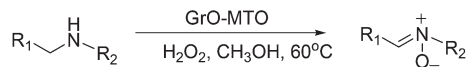
area, GrO has been employed as a remarkable support for catalytically active metal complexes, organic functionalities, and transition metal clusters for heterogenization of various catalysts for efficient chemical transformation.<sup>11–14</sup> Plenty of oxygen functional groups located on both sides of GrO sheets provide ample opportunities for excellent loading of these catalytically active moieties. Single or bimetallic nanoparticles such as Pt, Au–Pt, Pt–Pd, and Fe–Pt anchored on graphene based materials are found to exhibit good electro-catalytic activity in the oxidation of methanol, ethanol, and formic acid and in the reduction of oxygen in fuel cells.<sup>8–10</sup> Palladium nanoparticles grown on GrO have been identified as a highly active catalyst for the Suzuki–Miyaura coupling reaction.<sup>11</sup> Gold nanoparticles supported on GrO are found to facilitate reduction of *o*-nitroaniline to 1,2-benzenediamine with significantly higher catalytic activities than the corresponding gold nanoparticles, owing to induced electronic perturbations in the metallic component from the graphene support.<sup>12</sup> Recently, amino-grafted graphene has been developed as a basic catalyst for hydrolysis reactions with high catalytic activity.<sup>13</sup> Our group has recently reported the grafting of an oxo-vanadium Schiff base on GrO nanosheets for the oxidation of various alcohols under mild conditions. The developed catalyst was successfully reused for several runs without significant loss in its catalytic activity.<sup>14</sup> Such emerging developments on the heterogenization of various catalysts on GrO indicate immense potential for inexpensive and environmentally friendly organic transformation.

Oxidation of secondary amines to nitrones is one of the most valuable synthetic transformations, as nitrones are widely used intermediates in organic synthesis and also serve

<sup>a</sup>Chemical Sciences Division, CSIR-Indian Institute of Petroleum, Dehradun-248005, India. E-mail: [suman@iip.res.in](mailto:suman@iip.res.in), [opkhatri@iip.res.in](mailto:opkhatri@iip.res.in); Fax: +91-135-2660202; Tel: +91-135-2525788

<sup>b</sup>Analytical Sciences Division, CSIR-Indian Institute of Petroleum, Dehradun-248005, India

† Electronic supplementary information (ESI) available. See DOI: 10.1039/c3dt53421a



**Scheme 1** Oxidation of secondary amines in the presence of the GrO immobilized MTO catalyst.

as building blocks for the synthesis of active nitrogen containing compounds of biological importance.<sup>15</sup> Nitrones can readily be synthesized either by the condensation of carbonyl compounds with N-monosubstituted hydroxylamines or by oxidation of secondary amines or N,N-disubstituted hydroxylamines.<sup>16</sup> Among these two methods, oxidation of secondary amines to nitrones is more convenient and practical due to greater accessibility of secondary amines than hydroxylamines. A number of catalytic systems including  $\text{SeO}_2$ ,<sup>17</sup> metal-urea hydrogen peroxide (UHP-M, M = Mo, W),<sup>18</sup>  $\text{Na}_2\text{WO}_4\text{-H}_2\text{O}_2$ ,<sup>19</sup> tetra-*n*-propylammonium per-ruthenate (TPAP)/*N*-methylmorpholine N-oxide,<sup>20</sup>  $\text{R}_2\text{CuO}_2$ ,<sup>21</sup> flavin 4*a*-hydroperoxyflavin (4*a*-FLETOH),<sup>22</sup> Mg–Al layered double hydroxides- $\text{H}_2\text{O}_2$ <sup>23</sup> and nafion supported Mo-oxochloride- $\text{H}_2\text{O}_2$ <sup>24</sup> have been reported for oxidation of secondary amines to nitrones. However, most of the existing methods suffer from certain drawbacks such as lower catalytic activity and non-recyclability of the catalyst.

Rhenium oxo-complexes, particularly methyltrioxorhenium (MTO), has gained significant importance as a versatile catalyst for various organic transformations including oxidation reactions,<sup>25</sup> aldehyde olefination,<sup>26</sup> olefin metathesis,<sup>27</sup> etc. However, high cost and non-recyclability of the MTO catalyst are a major concern from environment and economic perspectives. Hence, significant effort has been made towards heterogenization of the MTO in order to combine the advantages of heterogeneous catalysts such as ease of product/catalyst separation and recyclability of the catalyst with the advantages of homogeneous catalysts, e.g. higher selectivity with efficient conversion. In this context, a number of supports such as silica, niobia, zeolites, polymers and ionic liquids have been utilized for heterogenization of the MTO catalyst.<sup>28–32</sup> However, in most of the cases, the obtained materials often show poor stability and activity, and suffer from extensive leaching problems.

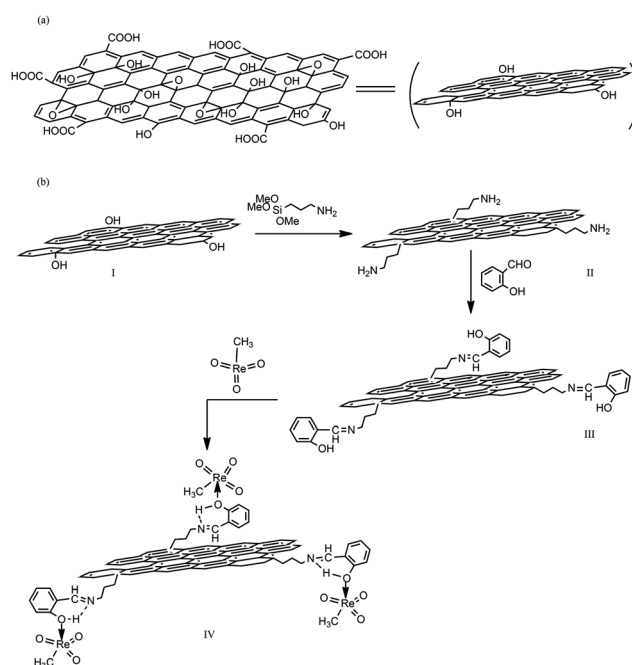
Herein, we report a very versatile and elegant approach to heterogenize the MTO catalyst on GrO nanosheets. The oxygen functionalities on GrO are targeted for stable and efficient anchoring of the MTO catalyst through Schiff base. The prepared heterogeneous material was found to be an efficient and recyclable catalyst for the oxidation of various secondary amines to nitrones using  $\text{H}_2\text{O}_2$  as a green oxidant (Scheme 1).

## Synthesis and characterization of the catalyst

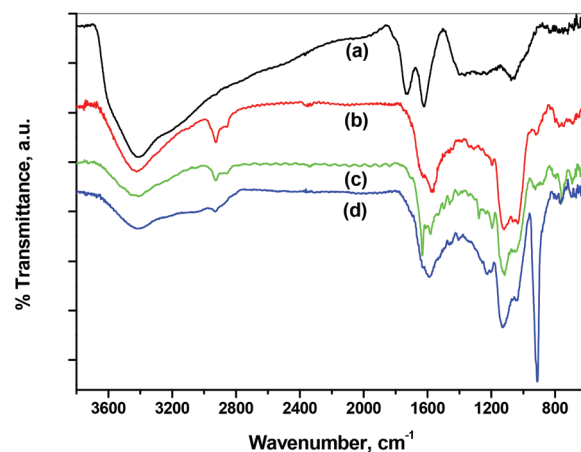
The GrO with its high specific surface area along with easily accessible ample oxygen functionalities decorated on both sides of the nanosheets shows great potential as a support

material for various catalysts. The heterogenization of the MTO catalyst was carried out targeting oxygen functionalities of the GrO using 3-aminopropyltrimethoxysilane (APTMS) and salicylaldehyde as couplers. The schematic illustration of immobilization of the MTO catalyst on GrO with all intermediate steps is shown in Scheme 2.

The developed heterogeneous catalyst is designated as GrO-MTO. The chemical changes that occurred during the immobilization of MTO-Schiff base on GrO were monitored by FTIR. Fig. 1 shows vibrational assessments of GrO, GrO-MTO, and intermediate products. The vibrational peaks with a strong intensity at 3397.5, 1723.8, 1224.9, and 1060.3  $\text{cm}^{-1}$ , attributed to stretching modes of O–H bonds, C=O, C–OH,



**Scheme 2** (a) Schematic model of GrO nanosheets and (b) individual steps for the preparation of the graphene oxide immobilized MTO catalyst.



**Fig. 1** FTIR spectra of (a) GrO, (b) GrO-APTMS, (c) GrO-SB, and (d) GrO-MTO.

and C–O–C, respectively, reveal the presence of hydroxyl, carboxyl, and epoxy groups in GrO.<sup>33,34</sup> Subsequent, covalent coupling of APTMS with hydroxyl groups of GrO was confirmed by the appearance of new vibrational signatures (a) in the region of 2800–3000  $\text{cm}^{-1}$  attributed to methylene and methyl groups, (b) at 3423.7 and 1573.2  $\text{cm}^{-1}$  attributed to amino groups, and (c) at 1121.5 and 1034.6  $\text{cm}^{-1}$  attributed to Si–O–Si and Si–O–C bonds, respectively.<sup>35</sup> The loading of salicylaldehyde on APTMS grafted GrO leads to Schiff base formation, which is corroborated by the appearance of new vibration signature at 1582.0  $\text{cm}^{-1}$  attributed to the C=N (imine) stretching mode.<sup>36</sup> The graphene immobilized MTO-Schiff complex, prepared by the co-ordination linkage between the Schiff base and MTO, was confirmed by the appearance of a very strong split vibration centred at 912.2  $\text{cm}^{-1}$  owing to Re=O asymmetric stretching. The asymmetric stretching attributed to Re=O shows a splitting of 10  $\text{cm}^{-1}$  (922 and 912  $\text{cm}^{-1}$ ) owing to the complex symmetry. The asymmetric stretching of the Re=O linkage in GrO-MTO is red-shifted compared to the non-coordinated MTO. The frequency shift reflects the donating capacity of the Schiff base ligand to the Lewis acid Re(VII) centre.<sup>35–37</sup> The stretching vibration of the imine (C=N) bond that appears at 1591.8  $\text{cm}^{-1}$  in the GrO-MTO catalyst is blue-shifted compared to the imine vibration (1582.0  $\text{cm}^{-1}$ ) in Schiff base immobilized GrO. Such shifts are associated with electron delocalization in the GrO-MTO catalyst.<sup>37,38</sup> The characteristic peaks extracted from the FTIR spectra of GrO, GrO-MTO, and intermediate products are separately given in Table S1 (ESI†) along with the vibrational assignment.

The thermal decomposition behaviour of the GrO and GrO-MTO catalyst was examined by thermogravimetric analysis. GrO shows ~6.4% weight loss in the range of 50–110 °C, evidently owing to evaporation of water molecules, which are trapped in the material. The second significant and major weight loss (34.6%) is observed in the range of 170–240 °C, due to thermal decomposition of labile oxygen functionalities (Fig. 1).<sup>14,39</sup> The GrO-MTO catalyst shows three mass losses up to 550 °C. The first abrupt mass loss (6%) up to 100 °C is owing to decomposition/sublimation of MTO. It is well established that MTO sublimates below 100 °C.<sup>40</sup> The second mass loss is in the range of 180–260 °C, attributed to the decomposition of (a) undigested oxygen carrying functionalities and (b) APTMS moieties, which have not participated in further chemical functionalization.<sup>39,41</sup> Then, another major mass loss is in the range of 360–470 °C owing to decomposition of the Schiff base (Fig. 2). The detailed TG-DTA patterns of both materials are shown in the ESI (Fig. S1 and S2†).

Micro-structural features and morphology of the as prepared graphene immobilized MTO-Schiff base catalyst were analyzed by FESEM and TEM. Fig. 3 shows twisted nanosheets in disordered phase with a lot of wrinkles and crumpling features of the GrO-MTO catalyst. These folded edges and protrusions owing to  $\text{sp}^3$  carbon in GrO-MTO carry the MTO-Schiff base complex on both sides of the GrO nanosheets, where reactants can easily access the catalytic sites and provide

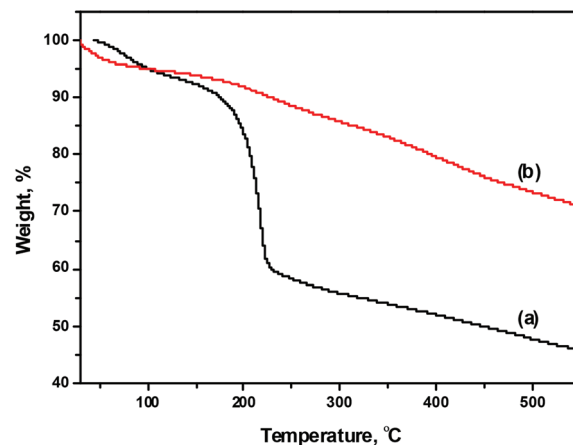


Fig. 2 TGA pattern of (a) GrO and (b) GrO-MTO catalyst over the temperature range of 30–550 °C.

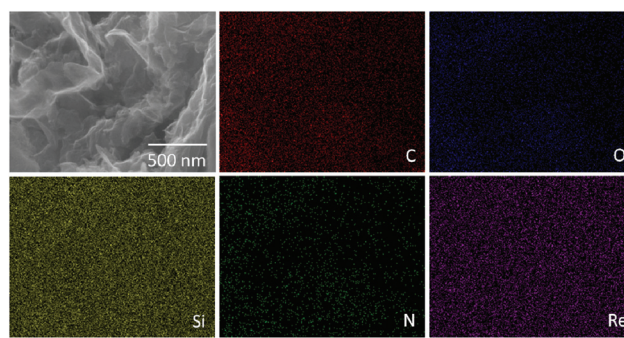


Fig. 3 FESEM image of the GrO-MTO catalyst and the corresponding elemental mapping images of carbon, oxygen, silicon, nitrogen and rhenium. Homogeneous distribution of silicon, nitrogen and rhenium indicates uniform loading of the MTO-Schiff base complex on GrO.

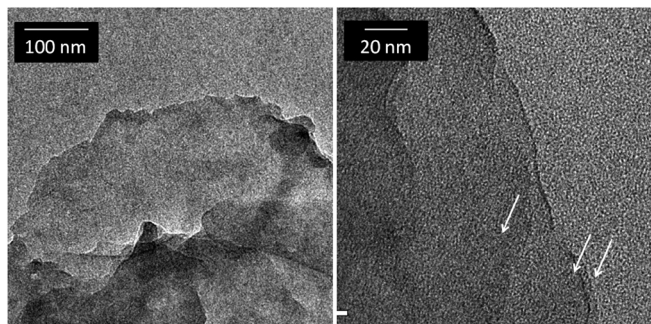


Fig. 4 TEM images of the GrO-MTO catalyst at low and high resolution.

efficient chemical transformation. The transmission electron microscopic images shown in Fig. 4 also reveal the nanoscopic features with layered structure of the GrO-MTO catalyst having very few numbers of layers (1–5) as indicated by white arrows. Such fine nanostructure of the MTO-GrO catalyst provides a high degree of active catalytic sites for efficient chemical transformation. The amorphous nature of the as-prepared catalyst is corroborated by the roughened surface of these nanosheets.

Elemental analysis based on EDS measurements provides detailed chemical information on the GrO-MTO catalyst. GrO is found to be mainly composed of carbon and oxygen along with traces of sulphur. The loading of the MTO-Schiff base complex on GrO changed the elemental composition with the introduction of rhenium, nitrogen and silicon, which are core elements of the immobilized MTO-Schiff base complex apart from carbon and oxygen. The reduced oxygen percentage in IV from 22.87% to 13.76% is attributed to the partial deoxygenation in GrO during the MTO-Schiff base grafting, which is corroborated by TGA. Further, energy-dispersive X-ray spectroscopy elemental mapping was performed to understand the distribution of the MTO-Schiff base complex on GrO. The thorough and uniform distribution of Re, N, and Si reveals that the MTO-Schiff base is uniformly immobilized on GrO as can be seen in Fig. 3, which is very important to execute an efficient catalytic chemical transformation. Furthermore, ICP-AES analysis of the catalyst provided 1.7 wt% Re in the synthesized heterogeneous material.

Furthermore, we have analyzed the GrO and GrO-MTO catalysts by UV-Vis spectroscopy to probe the chemical changes upon loading of the MTO complex (Fig. 5). The graphene oxide shows characteristic absorption at  $\sim 227$  nm owing to discrete units of  $sp^2$  bonded carbon. The loading of the MTO complex leads to significant changes in the absorption spectra of graphene oxide. An absorption peak at 227 nm in GrO was shifted to 254 nm in the GrO-MTO catalyst revealing conjugation between the support material and the catalytic material. Furthermore, the presence of  $n-\pi^*$  also supports the loading of the MTO catalyst on graphene oxide (GrO).

## Catalysis

The catalytic activity of the GrO-MTO was studied for the oxidation of various amines including aliphatic, aromatic and heterocyclic to the corresponding nitrones or N-oxides using hydrogen peroxide as an oxidant (Scheme 1). At first the oxidation of dibenzylamine with  $H_2O_2$  as an oxidant and methanol as a solvent was studied under various reaction conditions in order to optimize the reaction parameters. The results of

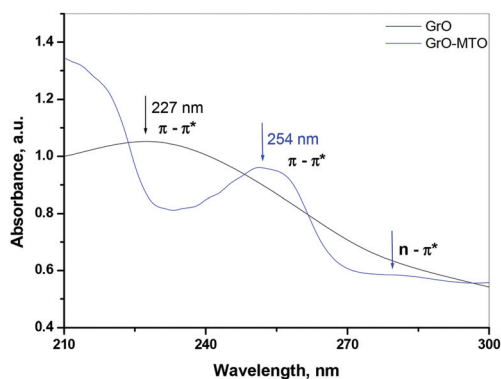
**Table 1** Optimization of reaction conditions for the oxidation of dibenzylamine into the nitrones<sup>a</sup>

Entry	Solvent	Cat. (1 mol%)	Temp./ °C	Time/ h	Conv. <sup>b</sup> (%)
1	Methanol	—	60	20	—
2	Methanol	IV	RT	24	5
3	Dichloromethane	IV	50	10	15
4	Benzene	IV	60	10	—
5	Acetonitrile	IV	60	12	18
6	Methanol	IV	60	2	45
7	Methanol	IV	60	4	69
8	Methanol	IV	60	6	100

<sup>a</sup> Reaction conditions: dibenzylamine (1 mmol),  $H_2O_2$  (3 mmol), catalyst (1 mol%). <sup>b</sup> Conversion (%) determined by GC-MS.

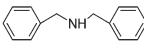
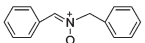
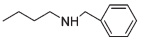
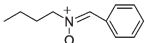
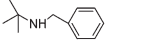
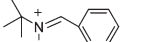
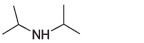
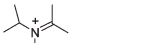
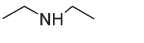
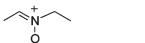
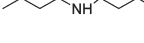
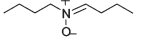
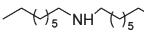
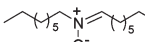
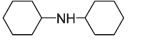
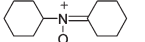
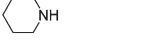
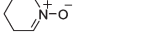
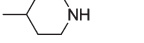
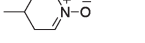

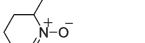
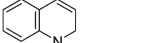
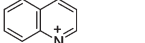


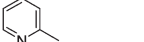





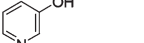
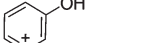


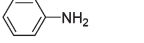
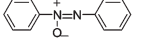
these chemical conversions under diverse conditions are summarized in Table 1. As shown, there was no reaction in the absence of a catalyst even after prolonged reaction time (Table 1, entry 1). Further, the reaction was found to be very slow at room temperature (Table 1, entry 2), whereas it could be completed within 6 h under refluxing conditions (Table 1, entry 8). Among the various solvents such as methanol, dichloromethane, benzene and acetonitrile studied, methanol was found to be the optimized reaction medium for the present transformation (Table 1, entries 3–8). To evaluate the effect of catalyst loading we performed the oxidation of dibenzylamine by varying the amount of catalyst from 1 to 5 mol% (Table 2, entry 1). As shown, the higher catalyst loading showed marginal improvement in the yield of the desired product. These findings indicated that the catalyst was equally efficient in lower loadings; therefore we have chosen a very fine amount of the catalyst (1 mol%) as the optimum concentration for the present transformation.

Thus, the optimized reaction conditions for the present reaction comprise the oxidation of dibenzylamine (1 mmol) with hydrogen peroxide (3 mmol) in the presence of the GrO-MTO catalyst (1 mol%, 0.01 mmol) in methanol under refluxing conditions. After completion of the reaction as analyzed by TLC ( $SiO_2$ ), the catalyst was easily separated by simple filtration and reused as such for subsequent runs. The filtrate was subjected to the usual workup to extract the corresponding nitrone. Further, the reaction was extended to a variety of amines including aliphatic, heterocyclic and aromatic secondary amines under the described reaction conditions. The results of these experiments are summarized in Table 2. In general the amines containing aromatic groups were found to be more reactive (Table 2, entries 1 and 2) than those of aliphatic and heterocyclic secondary amines (Table 2, entries 3–13). Further, the substrates containing bulky substituents were found to be less reactive and afforded poor product yield (Table 2, entries 3 and 4). We assume that the presence of bulky substituents causing steric hindrance might be responsible for the lower reactivity of these substrates. However, the



**Fig. 5** UV-Vis spectra of GrO and GrO-MTO.

Table 2 Oxidation of amines<sup>a</sup>

Entry	Reactant 1	Product 3	Time (h)	Conv. <sup>b</sup> (%)	Yield <sup>c</sup> (%)
1			6 6	87 92	85 90 <sup>d</sup>
2			5 6	95 89	92 <sup>e</sup> 85
3			6	56	53
4			8	54	—
5			8	88	85
6			7	85	82
7			8.5	80	76
8			6	74	72
9			8	77	75
10			6	82	80
11			6	85	82
12			6	60	55
13			8	80	76
14			8	85	82
15			8	95	90
16			10	65	58
17			10	72	68
18			12	70	67
19			4	99	97

<sup>a</sup> Reaction conditions: amine (1 mmol), 50% aq. H<sub>2</sub>O<sub>2</sub> (3 mmol), catalyst (1 mol%), methanol (5 ml) at 60 °C. <sup>b</sup> Conversion was determined by GC-MS. <sup>c</sup> Isolated yield. <sup>d</sup> Catalyst loading 2 mol%. <sup>e</sup> Catalyst loading 5 mol%.

reaction rate was found to decrease with increasing the alkyl chain length in aliphatic secondary amines (Table 2, entries 5–7). Heterocyclic secondary amines containing electron donating substituents were found to be more reactive (Table 2, entries 10 and 11) than the unsubstituted one (Table 2, entry 9). The oxidation of 1,2-dihydroquinoline under the described reaction conditions provided the corresponding quinoline N-oxide selectively without formation of any by-product (Table 2, entry 12).

Furthermore, we studied the oxidation of aromatic heterocyclic tertiary amines (pyridine and its derivatives) under the described experimental conditions. Pyridines containing electron donating groups were found to be more reactive (Table 2, entries 14 and 15) as compared to unsubstituted (Table 2, entry 13) and those having electron withdrawing substituents (Table 2, entry 16). Moreover, pyridines containing OH and  $-\text{COCH}_3$  groups selectively converted to the corresponding N-oxides without affecting the other functional groups in the substrates (Table 2, entries 17 and 18). In all cases, the conversion of the desired product was determined by GC-MS analysis. We also studied the oxidation of primary aromatic amines under the described reaction conditions. Surprisingly, aniline was selectively converted to azoxy-benzene (Table 2, entry 19), whereas substituted anilines did not produce any oxidation products and recovered as such at the end of the reaction.

Furthermore, the recycling of the GrO-MTO catalyst was examined by selecting the oxidation of dibenzylamine as the model reaction under optimized conditions. After completion of the reaction the catalyst could easily be recovered by filtration, dried and used for subsequent runs. The catalyst showed consistent activity up to three runs, which was gradually decreased for the subsequent runs. FTIR, TGA and ICP-AES analyses were used to assess the leaching of the MTO complex from the GrO support during the reaction. After three runs, there was little reduction in intensity of the  $\text{Re}=\text{O}$  stretch in FTIR spectra (Fig. S4†). This might be due to the partial leaching of the MTO complex from the developed heterogeneous catalyst during the reaction. Further, TGA results also revealed the loss of MTO from the graphene oxide support. There is approximately 1.5% mass loss difference between the fresh and residual catalysts. Additionally, in the ICP-AES analyses we found a reduced concentration of rhenium, *i.e.* 1.5 wt%, further indicating the leaching of MTO during the reaction.

The recyclability of the catalyst was checked for six runs (Table 3). The decreased product yield and longer reaction

time after three runs further supported the leaching of the MTO complex from the support during the reaction.

The developed catalyst was found to be superior to the existing supported catalysts. For example, oxidation of dibenzylamine with  $\text{H}_2\text{O}_2$  in the presence of tungstate-exchanged Mg–Al layered double hydroxides provided 60% yield of nitron in 5 h. Similarly, oxidation of benzaldehyde and benzylamine using UHP as an oxidant using Nafion immobilized  $\text{MoOCl}_2$  as a catalyst afforded 65% yield of the phenyl benzyl nitron in 4.5 h.

In summary, we have reported for the first time the immobilization of methyltrioxorhenium on the GrO *via* a chemical functionalization approach. Plenty of oxygen functionalities on GrO nanosheets facilitate efficient and uniform loading of MTO as revealed by FTIR and elemental mapping. The resulting functional material containing immobilized MTO has been successfully used as a catalyst in the oxidation of secondary amines to nitrones by using hydrogen peroxide as an oxidant. The best results were obtained while the reaction is carried out in methanol under refluxing conditions. The developed catalyst is easily recovered at the end of the reaction and recycled for several runs without any remarkable loss in catalytic activity.

## Grafting of MTO on graphene oxide

GrO, used as a nanostructural support material to immobilize the MTO-Schiff base complex, was prepared by harsh oxidation of graphite powder using the Hummers method.<sup>42</sup> Prior to chemical functionalization, graphite oxide was exfoliated into GrO with the aid of ultrasonication. Oxygen functionalities, especially hydroxyl and carboxyl groups placed on GrO, were targeted for grafting of the MTO-Schiff base complex, using 3-aminopropyltrimethoxysilane (APTMS) as a coupler. In a typical experiment, 1000 mg of GrO adequately dispersed in 400 ml toluene was refluxed with 4.0 ml of APTMS under a nitrogen atmosphere. After 24 hours, a black product of APTMS coated GrO was washed thoroughly with ethanol to remove physisorbed traces of APTMS. In the next step, 500 mg of APTMS coated GrO nicely dispersed in 250 ml ethanol was refluxed with 2400 mg salicylaldehyde under a nitrogen atmosphere in order to execute the reaction between amino groups of APTMS moieties and salicylaldehyde. In the final step, 500 mg of Schiff base immobilized GrO was dispersed in 150 ml of ethanol and then mixed with 500 mg ethanolic solution of MTO. The reaction mixture was stirred for 72 hours at ambient temperature under a nitrogen atmosphere to attain the MTO-Schiff base complex on graphene nanosheets. Then, the final product was washed with ethanol repetitively to remove the undigested content of MTO, and the dark black cake was dried in an oven. The developed black powder, so called graphene immobilized MTO, was used as a catalyst for the oxidation of various secondary amines to nitrones.

**Table 3** Results on recycling of the GrO-MTO catalyst<sup>a</sup>

Run	1	2	3	4	5	6
Time/h	6.0	6.0	6.0	6.5	6.5	6.5
Yield <sup>b</sup> (%)	85	85	84	82	82	78

<sup>a</sup> Conditions: dibenzylamine (1 mmol), 50% aq.  $\text{H}_2\text{O}_2$  (3 mmol), catalyst (1 mol%), methanol (5 ml) at 60 °C. <sup>b</sup> Isolated yield.

## Oxidation of secondary amines to nitrones

A 25 mL round bottom flask was charged sequentially with a catalyst, CH<sub>3</sub>OH (5 mL), and H<sub>2</sub>O<sub>2</sub> (3 mmol) and then stirred at room temperature for 10 minutes. Dibenzylamine (1 mmol) was added to the reaction mixture and the temperature of the reaction mixture was raised to 60 °C. Progress of the reaction with time was monitored by thin layer chromatography (SiO<sub>2</sub>). At the end of the reaction the catalyst was filtered over membrane filter paper and reused for subsequent runs. The filtrate thus obtained was treated with MnO<sub>2</sub> to decompose the excess H<sub>2</sub>O<sub>2</sub>. The treated reaction mixture was filtered to remove solid MnO<sub>2</sub> and then concentrated over rotavapor under reduced pressure. Organic layer was extracted with CH<sub>2</sub>Cl<sub>2</sub> and dried over anhydrous sodium sulfate. The product was purified by column chromatography over silica gel. Conversion of the product was determined by GC-MS analysis.

We kindly acknowledge the Director, IIP for his kind permission to publish these results. We are thankful to the Analytical Science Division of IIP for help in the analyses of the samples. For the HRTEM analysis, the DST unit of Nanoscience, IIT Chennai is kindly acknowledged.

## Notes and references

- B. F. Machado and P. Sherp, *Catal. Sci. Technol.*, 2012, **2**, 54–75.
- (a) D. R. Dreyer, S. Park, C. W. Bielawski and R. S. Ruoff, *Chem. Soc. Rev.*, 2010, **39**, 228–240; (b) O. C. Compton and S. T. Nguyen, *Small*, 2010, **6**, 711–723.
- C. Gomez-Navarro, J. C. Meyer, R. S. Sundaram, A. Chuvilin, S. Kurasch, M. Burghard, K. Kern and U. Kaiser, *Nano Lett.*, 2010, **10**, 1144–1148.
- (a) R. Muszynski, B. Seger and P. V. Kamat, *J. Phys. Chem. C*, 2008, **112**, 5263–5266; (b) T. N. Lambert, C. A. Chavez, B. Hernandez-Sanchez, P. Lu, N. S. Bell, A. Ambrosini, T. Friedman, T. J. Boyle, D. R. Wheeler and D. L. Huber, *J. Phys. Chem. C*, 2009, **113**, 19812–19823; (c) S. Choudhary, H. P. Mungse and O. P. Khatri, *J. Mater. Chem.*, 2012, **22**, 21032–21039.
- D. R. Dreyer, H. Jia and C. W. Bielawski, *Angew. Chem., Int. Ed.*, 2010, **49**, 6813–6816.
- D. R. Dreyer, H. Jia, A. D. Todd, J. Geng and C. W. Bielawski, *Org. Biomol. Chem.*, 2011, **9**, 7292–7295.
- M. Mirza-Aghayan, E. Kashef-Azara and R. Boukherroub, *Tetrahedron Lett.*, 2012, **53**, 4962–4965.
- M. Mirza-Aghayan, M. M. Taviana and R. Boukherroub, *Tetrahedron Lett.*, 2014, **55**, 342–345.
- S. Verma, H. P. Mungse, N. Kumar, S. Choudhary, S. L. Jain, B. Sain and O. P. Khatri, *Chem. Commun.*, 2011, **47**, 12673–12675.
- M. Mirza-Aghayana, R. Boukherroub, M. Nematia and M. Rahimifard, *Tetrahedron Lett.*, 2012, **53**, 2473–2475.
- (a) Y. Hu, H. Zhang, P. Wu, H. Zhang, B. Zhou and C. Cai, *Phys. Chem. Chem. Phys.*, 2011, **13**, 4083–4094; (b) C. V. Rao, C. R. Cabrera and Y. Ishikawa, *J. Phys. Chem. C*, 2011, **115**, 21963–21970; (c) S. Guo, S. Dong and E. Wang, *ACS Nano*, 2010, **4**, 547–555; (d) S. Guo and S. Sun, *J. Am. Chem. Soc.*, 2012, **134**, 2492–2495.
- (a) G. M. Scheuermann, L. Rumi, P. Steurer, W. Bannwarth and R. Mulhaupt, *J. Am. Chem. Soc.*, 2009, **131**, 8262–8270; (b) J. Huang, L. Zhang, B. Chen, N. Ji, F. Chen, Y. Zhang and Z. Zhang, *Nanoscale*, 2010, **2**, 2733–2738.
- C. Yuan, W. Chen and L. Yan, *J. Mater. Chem.*, 2012, **22**, 7456–7460.
- H. P. Mungse, S. Verma, N. Kumar, B. Sain and O. P. Khatri, *J. Mater. Chem.*, 2012, **22**, 5427–5433.
- (a) K. B. G. Torrsell, *Nitrile Oxides, Nitrones and Nitronates in Organic Synthesis*, VCH Publishers, New York, 1988; (b) G. Tennant, in *Comprehensive Organic Chemistry*, ed. D. H. R. Barton and W. D. Ollis, Pergamon Press, New York, 1979, vol. 2; (c) A. Padwa, *1,3-Dipolar Cycloaddition Chemistry*, Wiley, New York, 1984, vol. 2, p. 83; (d) P. N. Confalone and E. M. Huie, *The [3 + 2] Nitron-Olefin Cycloaddition Reaction. In Organic Reactions*, Wiley, New York, 1988, vol. 36.
- E. Breuer, in *The Chemistry of Amino, Nitroso and Nitro Compounds and Their Derivatives*, ed. S. Patai, Wiley, New York, 1982, p. 459.
- S. I. Murahashi and T. Shiota, *Tetrahedron Lett.*, 1987, **28**, 2383–2386.
- E. Marcantoni, M. Petrini and O. Polimanti, *Tetrahedron Lett.*, 1995, **36**, 3561–3562.
- S. I. Murahashi, H. Mitsui, T. Shiota, T. Tsuda and S. Watanabe, *J. Org. Chem.*, 1990, **55**, 1736–1744.
- A. Goti, F. D. Sarlo and M. Romani, *Tetrahedron Lett.*, 1994, **35**, 6571–6574.
- R. W. Murray and M. Singh, *J. Org. Chem.*, 1990, **55**, 2954–2957.
- (a) S. Ball and T. C. Bruice, *J. Am. Chem. Soc.*, 1980, **102**, 6498–6503; (b) S. I. Murahashi, T. Oda and Y. Masui, *J. Am. Chem. Soc.*, 1989, **111**, 5002–5003.
- B. M. Choudary, B. Bharathi, Ch. Venkat Reddy and M. Lakshmi Kantam, *Green Chem.*, 2002, **4**, 279–284.
- B. Singh, S. L. Jain, P. K. Khatri and B. Sain, *Green Chem.*, 2009, **11**, 1941–1944.
- (a) W. A. Herrmann, R. W. Fischer and D. W. Marz, *Angew. Chem., Int. Ed. Engl.*, 1991, **30**, 1638–1641; (b) Z. Zhu and J. H. Espenson, *J. Org. Chem.*, 1995, **60**, 7728–7732; (c) W. Adam, W. A. Herrmann, C. R. Saha-Moller and M. Shimizu, *J. Mol. Catal. A: Chem.*, 1995, **97**, 15–20; (d) R. Saladino, V. Neri, E. Mincione, S. Marini, M. Coletta, C. Fiorucci and P. Filippone, *J. Chem. Soc., Perkin Trans.*, 2000, 581–586; (e) W. Adam, W. A. Herrmann, J. Lin and C. R. Saha-Moller, *J. Org. Chem.*, 1994, **59**, 8281–8283; (f) W. Adam, W. A. Herrmann, J. Lin, C. R. Saha-Moller, R. W. Fischer and J. D. G. Correia, *Angew. Chem., Int. Ed. Engl.*, 1994, **33**, 2475–2477; (g) M. M. Abu-Omar and J. H. Espenson, *J. Am. Chem. Soc.*, 1995, **117**, 272–280.

- 26 W. A. Herrmann and M. Wang, *Angew. Chem., Int. Ed. Engl.*, 1991, **30**, 1641–1643.
- 27 W. A. Herrmann, W. Wagner, U. N. Flessner, U. Volkhardt and H. Komber, *Angew. Chem., Int. Ed. Engl.*, 1991, **30**, 1636–1638.
- 28 T. J. Wang, D. C. Li, J. H. Bai, M. Y. Huang and Y. Y. Jiang, *J. Macromol. Sci., Pure Appl. Chem.*, 1998, **A35**, 531–538.
- 29 A. B. Bouh and J. H. Espenson, *J. Mol. Catal. A: Chem.*, 2003, **206**, 37–51.
- 30 W. Adam, C. R. Saha-Möller and O. Weichold, *J. Org. Chem.*, 2000, **65**, 2897–2899.
- 31 R. Saladino, V. Neri, F. Cardona and A. Goti, *Adv. Synth. Catal.*, 2004, **346**, 639–647.
- 32 R. Bernini, A. Coratti, G. Fabrizi and A. Goggiamani, *Tetrahedron Lett.*, 2003, **44**, 8991–8994.
- 33 A. Stuart, *Infrared Spectroscopy: Fundamentals and Applications*, J. Wiley, Chichester, West Sussex, England, Hoboken, NJ, 2004.
- 34 (a) D. Pan, S. Wang, B. Zhao, M. Wu, H. Zhang, Y. Wang and Z. Jiao, *Chem. Mater.*, 2009, **21**, 3136–3142; (b) J. I. Paredes, S. Villar-Rodil, A. Martinez-Alonso and J. M. D. Tascon, *Langmuir*, 2008, **24**, 10560–10564; (c) R. Pena-Alonso, F. Rubio, J. Rubio and J. L. Oteo, *J. Mater. Sci.*, 2007, **42**, 595–603; (d) R. M. Pasternack, S. R. Amy and Y. J. Chabal, *Langmuir*, 2008, **24**, 12963–12971.
- 35 Y. Gao, Y. Zhang, C. Qiu and J. Zhao, *Appl. Organomet. Chem.*, 2011, **25**, 54–60.
- 36 M. Santos, F. E. Kuhn, W. M. Xue and E. Herdtweck, *J. Chem. Soc., Dalton Trans.*, 2000, 3570–3574.
- 37 D. Nunes, M. Pillinger, A. A. Valente, I. S. Goncalves, J. Rocha, P. Ferreira and F. E. Kuhn, *Eur. J. Inorg. Chem.*, 2002, 1100–1107.
- 38 M. Zhou, J. Zhao, J. Li, S. Yue, C. Bao, J. Mink, S. Zhang and F. E. Kuhn, *Chem. – Eur. J.*, 2007, **13**, 158–166.
- 39 S. Stankovich, D. A. Dikin, R. D. Piner, K. A. Kohlhaas, A. Kleinhammes, Y. Jia, Y. Wu, S. T. Nguyen and R. S. Ruoff, *Carbon*, 2007, **45**, 1558–1565.
- 40 W. A. Herrmann, W. M. Wachter, F. E. Kühn and R. W. Fischer, *J. Organomet. Chem.*, 1998, **553**, 4432452.
- 41 S. Gupta, P. C. Ramamurthy and G. Madras, *Polym. Chem.*, 2011, **2**, 221–228.
- 42 W. S. Hummers and R. E. Offeman, *J. Am. Chem. Soc.*, 1958, **80**, 1339.